On the Power-Weighted Efficiency of Multimode Powertrains: A Case Study on a Two-Mode Hybrid System

On the Power-Weighted Efficiency of Multimode Powertrains: A Case Study on a Two-Mode Hybrid System

Antonio Tota(✉), Enrico Galvagno, and Mauro Velardocchia

Politecnico di Torino, Turin, Italy
antonio.tota@polito.it

Abstract. Multimode powertrains represent one of the most versatile solutions for hybrid electric vehicles where multiple power sources are integrated with aim of improving fuel economy and reducing pollutants emission in every operating condition. Some hybrid powertrain designs feature multiple planetary gear sets whose components can be directly driven by the powertrain actuators (electric motor or thermal engine) or can be connected through clutches and brakes. The advantages due to the availability of multiple modes are mitigated by the increase of production costs and complexity because of the higher number of components required if compared with the single mode solutions. A numerical methodology is adapted from the literature to analyze, categorize, and compare each distinct working configuration. The energy consumption of each powertrain configuration is then evaluated through the power-weighted efficiency concept whose formulation normalize the contribution from each power source. This paper aims at extending the methodology to investigate the operating range for each powertrain configuration to always achieve the maximum efficiency. The methodology is then applied to the realistic case study of the EVT 2-Mode Hybrid System.

Keywords: SDG11 · Multimode powertrains · Hybrid vehicles · Planetary gears · EVT 2-mode hybrid system

1 Introduction

The market of passenger cars is going through a challenging period where fuel economy and emission reduction represent the main driving factors for the definition of product portfolio by the car makers to satisfy the sustainable development goals set by the United Nations [1]. Hybrid powertrains are certainly among the most supported solutions adopted by car manufactures to minimize the fuel consumption. Indeed, the powertrain efficiency can be improved by introducing one or more electric motors/generators, in addition to the conventional internal combustion engine. The power flow through the powertrain components is defined according to three basic architectures: series, parallel, and series–parallel (power-split) [2, 3]. Within the last category, the Electrically Variable Transmission (EVT) or Electric Continuously Variable Transmission (E-CVT) stands out for their performance and operating efficiency, also favored by a more efficient use of the

G. Quaglia et al. (Eds.): I4SDG 2021, MMS 108, pp. 1–10, 2022.
https://doi.org/10.1007/978-3-030-87383-7_56

engine, as described by [4, 5]. A multimode hybrid powertrain enables different working modes, e.g. series, parallel, input split, output split, compound split, according to the state of clutches and brakes. This solution ensures grater adaptability to different vehicle operations and fully realizes the powertrain potential to achieve both better fuel economy and improved drivability, as compared to conventional vehicles. An automated procedure to analyze and categorize the whole set of the multimode powertrains is proposed by [6, 7] meanwhile a comparative study of multimode powertrains with different numbers of planetary gear sets (PGS) is carried out by [8] where it is demonstrated that three or more PGS does not show a significant fuel economy improvement for passenger cars with respect to the two PGS configurations. Once the powertrain architecture is defined and all the feasible modes are identified, a methodology to choose the correct mode to achieve the best possible fuel economy for each operating condition is required. Among the most studied and implemented solutions there are the equivalent consumption minimization strategy (ECMS) [9, 10], the Pontryagin's minimum principle (PMP) [11, 12] and the dynamic programming (DP) [13] which are all optimization-based algorithms to satisfy a prescribed cost function or performance index. The DP and the PMP methods are the most reliable solutions, but the DP requires a high computational power meanwhile the PMP may suffer from numerical convergence problems. The ECMS represents an instantaneous suboptimal solution for the fuel economy optimization problem, but it needs a specific tuning for the equivalence factor calculation. To overcome these limits, a suboptimal energy management strategy, named power-weighted efficiency analysis for rapid sizing (PEARS) is proposed by [6], whose results are similar to the DP optimal solution but much more convenient in terms of computational burden. In this paper, the PEARS method is applied to a two-mode hybrid system developed by General Motors [14], whose dynamics is also analyzed in [15] for different driving conditions. The paper is organized as follows: Sect. 2 describes the automated procedure to build and classify the dynamics model of each powertrain mode; the description of the power-weighted efficiency algorithm is carried out in Sect. 3; the results for the two-mode hybrid system are shown in Sect. 4 meanwhile the conclusions are drawn in Sect. 5.

2 Multimode Powertrain Model

An example of a multimode hybrid powertrain featuring two planetary gear sets, an internal combustion engine (ICE), two electric motors/generators (MGs), a clutch and a brake, is shown in Fig. 1. Given a transmission architecture with n PGS, the total number of nodes (a node is a ring, a solar or a carrier) is equal to $3n$. Each PGS provides two degrees-of-freedom (dofs) meanwhile each clutch engagement removes one degree-of-freedom (dof) by constraining the motion between two PGS's elements or by connecting one PGS element to the powertrain chassis (grounding clutch). By considering a number n of PGS and a number q of engaged clutches, each powertrain configuration owns a total number of $2n - q$ degrees-of-freedom. The example reported in Fig. 1 shows a total number of $n = 2$ PGS with 1 rigid connections between the carriers of the two PGS and the presence of 2 clutches. If one clutch is engaged, then the powertrain has two degrees-of-freedom ($q = 2$).

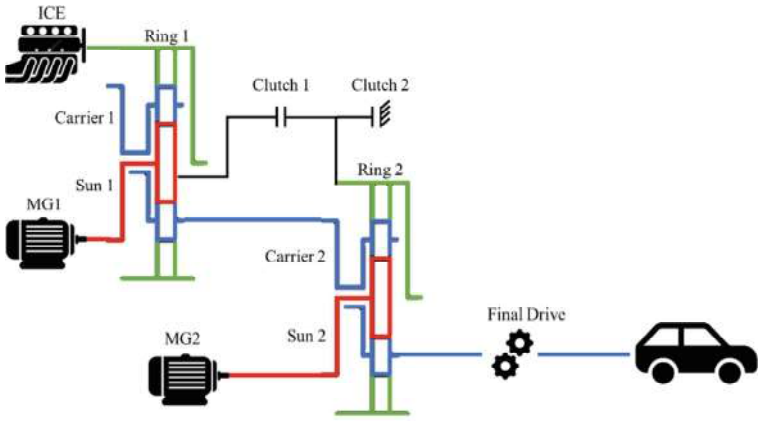

Fig. 1. Scheme of the powertrain architecture in the EVT 2-mode Hybrid System.

Note that the system dofs must be within the range of one to the number of the power components (ICE and/or MGs) so that the vehicle is controllable and drivable. The following sections describe the automated modelling procedure introduced by [7] to elaborate the powertrain dynamic equations for each architecture configuration.

2.1 Dynamics Model

The powertrain dynamics with no connections among PGS nodes is described by:

$$\boldsymbol{A_0 x_0} = \boldsymbol{u_0} \tag{1}$$

Where $\boldsymbol{x_0} = \left[\dot{\Omega}_0 \; \boldsymbol{F}\right]^T$ is the generalized coordinate vector, $\dot{\Omega}_0 = \left[\dot{\omega}_{c,1} \; \dot{\omega}_{s,1} \; \dot{\omega}_{r,1} \; \ldots \; \dot{\omega}_{c,n} \; \dot{\omega}_{s,n} \; \dot{\omega}_{r,n}\right]^T$ is the angular acceleration vector (dimension of $3n$x 1) which includes the angular acceleration of the carrier ($\dot{\omega}_{c,i}$), the sun ($\dot{\omega}_{s,i}$) and the ring ($\dot{\omega}_{r,i}$), respectively, for the $i_{th} = 1 : n$ PGS. The vector $\boldsymbol{F}$ (dimension of nx 1) contains the internal forces F_i between the ring and the pinions gears teeth of the i_{th} PGS. $\boldsymbol{u_0} = \left[\boldsymbol{T} \; 0\right]^T$ represents the $4n$x 1 generalized input vector where the elements of $\boldsymbol{T} = \left[T_{load} \; T_{eng} \; T_{MG1} \; \ldots \; T_{MGk}\right]^T$ (dimension of $3n \times 1$) are the torques applied to the transmission, e.g. the output transmission torque T_{load} obtained from the vehicle motion resistances, the ICE torque T_{eng}, and the MGs torques T_{MG1}, T_{MG2}, …, T_{MGk}, where k is the total number of MGs. The first $3n$ equations of Eq. 1 describe the torsional dynamic equilibrium for each PGS node meanwhile the last n equations report the PGS kinematic relation among the ring, the solar and the carrier angular speeds: $\omega_{s,i} r_{s,i} + \omega_{r,i} r_{r,i} = \omega_{c,i}\left(r_{s,i} + r_{r,i}\right)$, where $r_{r,i}$ and $r_{s,i}$ are the radius of the ring and the solar, respectively. The matrix $\boldsymbol{A_0}$ has dimension of $4n$x $4n$ and includes all the inertial and geometric parameters of the transmission:

$$\boldsymbol{A_0} = \begin{bmatrix} \boldsymbol{J} & \boldsymbol{B} \\ \boldsymbol{B^T} & 0 \end{bmatrix} \tag{2}$$

Where the matrix $\boldsymbol{J}$ is a $3n \times 3n$ diagonal matrix whose elements are the total torsional moment of inertia of the powertrain components connected to each PGS node. The matrix $\boldsymbol{B}$ is a $3n \times n$ whose elements of the i_{th} column are $-r_{r,i}$, $-r_{s,i}$ or $r_{r,i} + r_{s,i}$ if the corresponding $\boldsymbol{A_0}$ raw refers to the torsional dynamic equilibrium of the ring, the solar or the carrier, respectively. The remaining elements of the matrix $\boldsymbol{B}$ are set to zero.

To obtain the dynamics of the system after the engagement of q clutches, the transition matrices $\boldsymbol{C}$ and $\boldsymbol{D}$ are introduced:

$$\underbrace{\left(\boldsymbol{C}\boldsymbol{A_0}\boldsymbol{C}^{\boldsymbol{T}}\right)}_{\boldsymbol{A}} \underbrace{(\boldsymbol{D}\boldsymbol{x_0})}_{\boldsymbol{x}} = \underbrace{(\boldsymbol{C}\boldsymbol{x_0})}_{\boldsymbol{u}} \tag{3}$$

Matrices $\boldsymbol{C}$ and $\boldsymbol{D}$ are initialized as a $4n \times 4n$ identity matrices $\boldsymbol{I}_{4n}$ whose rows are modified based on the position of the PGS nodes in Eq. 1 connected through the engagement of each clutch (see [6–8] for further details). It is important to remark that this mathematical model does not include the transmission nonlinearities such as the gear backlashes, whose presence may affect the powertrain torsional dynamics in specific conditions [16].

2.2 Powertrain Modes Classification

The engagement of q clutches lead to multiple powertrain modes whose dynamic behavior is described by Eq. 3. However, some modes may share identical dynamic equations, thus resulting in redundant powertrain configurations, or some may include infeasible solutions where the vehicle is not powered by any powertrain components. It is relevant to identify and remove both redundant and infeasible powertrain modes.

The first step to eliminate these modes, consists of inverting the matrix $\boldsymbol{A}$, thus relating the torques $\boldsymbol{T}$ to the angular acceleration of each PGS node:

$$\boldsymbol{x} = \boldsymbol{A}^{-1}\boldsymbol{u} \tag{4}$$

However, not every element in $\boldsymbol{x}$ is useful for the powertrain modes analysis and classification, e.g. the dynamics of the free nodes, that are not connected to a power components or to the vehicle, is not of interest. By considering the useful part of vector $\boldsymbol{x}$, named in the following with the vector $\boldsymbol{x}^*$, the inverse dynamic equation is obtained:

$$\boldsymbol{x}^* = \left[\, \dot{\omega}_{out}\ \dot{\omega}_{eng}\ \dot{\omega}_{MG1}\ \ldots\ \dot{\omega}_{MGk} \,\right]^T = \boldsymbol{A}^*\boldsymbol{T} \tag{5}$$

The size of $\boldsymbol{x}^*$ and $\boldsymbol{T}$ vectors is $(m+1)$x1, where m is the number of the power components. The size of $\boldsymbol{A}^*$ is then $(m+1) \times (m+1)$. By analyzing each row of the resulting matrix $\boldsymbol{A}^*$, it is possible to remove the unfeasible configurations (i.e. a component not connected to the rest of powertrain) and the redundant modes with identical matrix $\boldsymbol{A}^*$ (see [6–8] for further details).

3 Power-Weighted Efficiency

The selection of the most suitable powertrain mode, for each vehicle operating condition, relies on the minimum energy consumption criterion. The methodology adopted in this

paper to solve the energy loss minimization problem is the power-weighted efficiency analysis for rapid sizing (PEARS) proposed by [7].

The PEARS concept is based on the calculation of the power-weighted efficiency of each powertrain mode as function of the vehicle operating conditions, defined by the load torque T_{load} applied to the transmission output shaft and the desired vehicle speed V. The evaluation of the power-weighted efficiency for each powertrain mode requires the calculation of the output power requested to each powertrain component as well as its individual efficiency. Given T_{load} and V, the transmission output acceleration is calculated as:

$$\dot{\omega}_{out,ref} = \frac{\tau_F}{MR_W}\left(T_{out}\frac{\tau_F}{R_W} - Mgf_0 - \frac{1}{2}\rho C_x S_F V^2\right) \tag{6}$$

Where M is the vehicle mass, τ_F is the transmission final drive ratio, R_W is tire rolling radius, g is the gravitational acceleration, f_0 is the constant tire rolling resistance coefficient, ρ is the air density, C_x is the aerodynamic drag coefficient and S_F the vehicle frontal area. For each powertrain mode, characterized by a matrix $\boldsymbol{A}^*$, it is possible to search for the torque distribution $\boldsymbol{T}$ such that $\dot{\omega}_{out} = \dot{\omega}_{out,ref}$ through Eq. 6. The output transmission speed is calculated as $\omega_{out} = V\frac{\tau_F}{R_W}$. If the powertrain mode has one dof, the angular speed of each powertrain component is calculated through the PGS kinematic relation constrained by the engagement of q clutches. If the powertrain mode has two or more degrees-of-freedom, one or more angular speeds must be imposed, e.g. the ICE speed. Knowing the vector $\boldsymbol{T}$ and the angular speeds, it is possible to evaluate the output power and the efficiency of each powertrain component. By assuming $k = 2$ MGs, the electric power produced by the generators P_G, and the electric power absorbed by the motors P_M is then calculated in Table 1, together with their correspondent efficiencies η_G and η_M.

Table 1. Electric power and efficiency for the electric power absorbed and generated

IF	P_G	P_M	η_G	η_M
$P_{MG1} \leq 0$ $P_{MG2} \leq 0$	$-P_{MG1}\eta_{MG1} - P_{MG2}\eta_{MG2}$	0	$\frac{P_{MG1}\eta_{MG1}+P_{MG2}\eta_{MG2}}{P_{MG1}+P_{MG2}}$	0
$P_{MG1} \leq 0$ $P_{MG2} \geq 0$	$-P_{MG1}\eta_{MG1}$	$-\frac{P_{MG2}}{\eta_{MG2}}$	η_{MG1}	η_{MG2}
$P_{MG1} \geq 0$ $P_{MG2} \leq 0$	$-P_{MG2}\eta_{MG2}$	$-\frac{P_{MG1}}{\eta_{MG1}}$	η_{MG2}	η_{MG1}
$P_{MG1} \geq 0$ $P_{MG2} \geq 0$	0	$-\frac{P_{MG1}}{\eta_{MG1}} - \frac{P_{MG2}}{\eta_{MG2}}$	0	$\frac{P_{MG1}\eta_{MG1}+P_{MG2}\eta_{MG2}}{P_{MG1}+P_{MG2}}$

Where P_{MG1}, P_{MG2} are the output power of the two MGs and η_{MG1}, η_{MG2} their correspondent efficiencies.

The demanded power at the transmission output can be fed by two energy sources: the battery and the fuel tank. In the generic scheme of Fig. 2, the engine output power $P_e =$

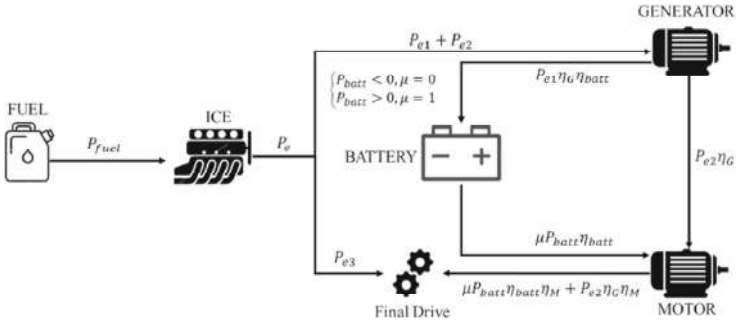

Fig. 2. Generic scheme of the power flow for a hybrid powertrain.

$T_e\omega_e$ can be split into three contributions: the engine power P_{e1} that flows to the battery through the generator, the engine power P_{e2} that flows to the electric motor through the generator and the engine power P_{e3} that directly flows to transmission output shaft. P_{batt} and P_{fuel} represent the battery power and the fuel power consumed, respectively. If $P_G > P_M$, the additional power is used to charge the battery ($\mu = 0$): $P_{e3} = P_e - \frac{P_G}{\eta_G}$, $P_{e2}\eta_G = P_M$, $P_{e1}\eta_G = P_G - P_{e2}\eta_G$ and $P_{batt} = -P_{e1}\eta_G\eta_{batt}$. Otherwise, if $P_G < P_M$, the battery energy is consumed ($\mu = 1$): $P_{batt} = (P_M - P_G)/\eta_{batt}$, $P_{e2}\eta_G = P_G$, $P_{e1}\eta_G = 0$, and $P_{e3} = P_e - \frac{P_G}{\eta_G}$. The battery efficiency η_{batt} is evaluated by considering a simple circuit model (see [17]):

$$\eta_{batt} = 1 - \frac{R_{batt}I_{batt}^2}{V_{oc}I_{batt}} \tag{7}$$

where I_{batt} is the current through the battery circuit:

$$I_{batt} = \frac{V_{oc} - \sqrt{V_{OC}^2 - 4R_{batt}|P_M - P_G|}}{2R_{batt}} \tag{8}$$

The resistance of the battery circuit R_{batt} and the battery open circuit voltage V_{oc} are considered as constant quantities.

Finally, the power-weighted efficiency η_{HEV} is evaluated as:

$$\eta_{HEV} = \frac{\frac{P_{e1}\eta_G\eta_{batt}}{\eta_{e,max}\eta_{G,max}} + \frac{P_{e2}\eta_G\eta_M}{\eta_{e,max}\eta_{G,max}\eta_{M,max}} + \frac{P_{e3}}{\eta_{e,max}} + \frac{\mu P_{batt}\eta_{batt}\eta_M}{\eta_{M,max}}}{P_{fuel} + \mu P_{batt}} \tag{9}$$

where $\eta_{e,max}$, $\eta_{G,max}$, and $\eta_{M,max}$ are the maximum achievable efficiencies for the engine, the generator, and the motor, respectively. This formulation allows to normalize the efficiencies from different type of power sources, without penalizing the engine operation even if $\eta_{e,max}$ is much lower than $\eta_{G,max}$, and $\eta_{M,max}$.

For each combination of T_{load} and V, a multiple solution for the torque distribution vector $\boldsymbol{T}$ that satisfy $\dot{\omega}_{out} = \dot{\omega}_{out,ref}$ may exists and two different criteria are defined to discriminate the preferred solution. For the Charge-Sustaining criterion, the objective is to keep constant the battery state of charge, and the torque distribution $\boldsymbol{T}$ that guarantees

the minimum battery power P_{batt} is selected (only if $\dot{\omega}_{out,ref} \geq 0$). Otherwise, in case of a Charge-Depleting criterion, the use of electric motors is prioritized over the engine, and a torque distribution $\boldsymbol{T}$ that provides the maximum efficiency η_{HEV} is preferred. It is important to remark that the vehicle braking is only entrusted to the electric generators, thus not considering the presence of a conventional hydraulic braking system (see [18] for further details).

4 Case Study: EVT 2-Mode Hybrid System

The general methodology described in the previous sections is then applied to the specific case of the EVT 2-mode hybrid system. The powertrain architecture is shown in Fig. 1, where $n = 2$ PGS are connected in series. The engine and the first electric motor MG1 are installed on the ring and the sun of the first PGS, respectively. The second electric motor MG2 and the transmission output shaft are connected to the sun and the carrier of the last PGS, respectively. A rigid connection constrains the carriers of the two PGS and the presence of two clutches enables the activation of the input split (clutch 1 engaged) or the compound split (clutch 2 engaged) hybrid modes. The total number of dofs is two for both powertrain modes, so the engine speed ω_{eng} is chosen as second degree of freedom together with ω_{out}. The list of vehicle parameters used for the calculation of the η_{HEV} for each powertrain mode is also shown in Table 2.

Table 2. List of vehicle parameters used for the η_{HEV} calculation

M	1600 kg	ρ	1.2 kg/ m^3
R_W	0.34 m	τ_F	3.02
f_0	0.01	$r_{r,1}, r_{s,1}, r_{r,2}, r_{s,2}$	8, 5, 8, 5 cm
C_x	0.26	$J_{out}, J_{eng}, J_{MG1}, J_{MG2}$	20.28, 0.2, 0.05, 0.05 kg m^2
S_F	2 m^2	$J_{r,1}, J_{c,1}, J_{s,1}, J_{r,2}, J_{c,2}, J_{s,2}$	0.08, 0.06, 0.05, 0.08, 0.06, 0.05 kg m^2

The torque and efficiency characteristics of the engine and the two electric motors, reported in Fig. 3, are obtained from a commercial software usually adopted for modelling and simulating the behavior of hybrid vehicles.

The matrix $\boldsymbol{A}^*$ is calculated for both the input split and the compound split powertrain modes, thus obtaining the dynamic relation between each powertrain component acceleration to the torque distribution among the engine, the two electric motors and the vehicle resistance load. A 2D grid of values for T_{load} and V is selected as representative for the whole vehicle operating range, and the procedure described in the previous section is then applied to evaluate the torque and angular speed of each powertrain component. The results are shown for the compound split mode with the charge-sustaining and the charge-depleting criteria in Fig. 4, where the power flow among the four components is evaluated for each grid point of the vehicle operating range.

The Charge-Sustaining objective in Fig. 4 (left) is achieved by a P_{batt} almost null when $\dot{\omega}_{out,ref} \geq 0$ (above the black line representing the vehicle motion resistance at

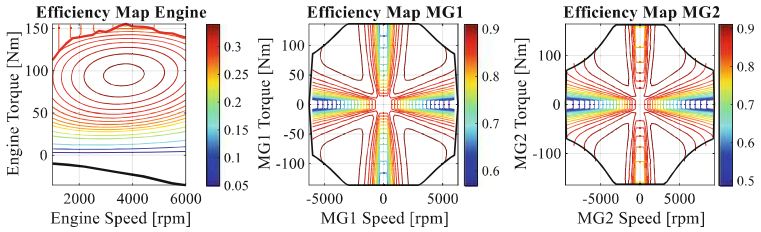

Fig. 3. Efficiency maps for the engine (left), the MG1 (center) and the MG2 (right) of the EVT 2-mode hybrid system

constant speed), so that the state of charge of the battery is maintained at a certain level while accelerating. However, this solution does not exploit the potential of the electric power stored in the battery, thus requiring a frequent intervention of the engine with a consequent reduced power-weighted efficiency. On the other hand, the charge-depleting solution in Fig. 4 (right) is much more oriented towards the minimization of the power losses, relying on the electric energy stored in the battery and limiting the engine intervention within its operating range of maximum efficiency. Similar conclusions can be drawn also for the input slip mode.

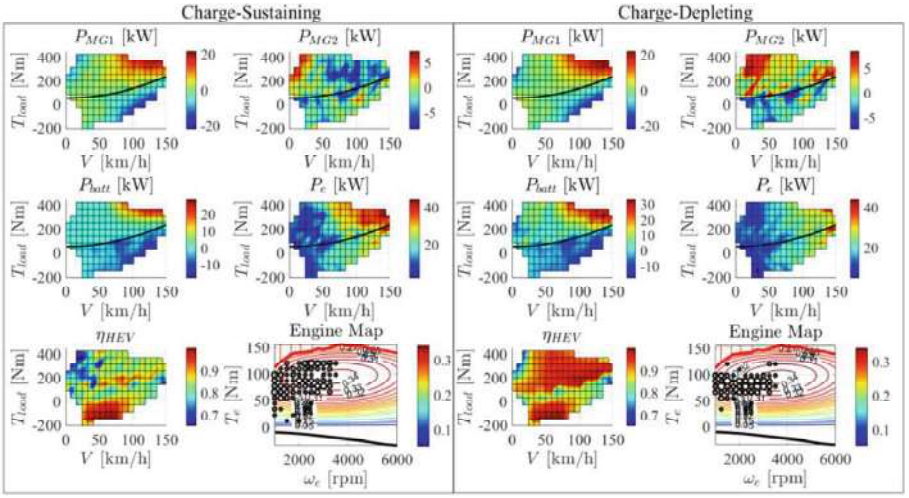

Fig. 4. MG1 power, MG2 power, battery power, ICE power, power-weighted efficiency, and map with engine working conditions (black circles) for the compound split mode with the charge-sustaining (left) and charge-depleting (right) torque distribution criteria.

Finally, for each combination of T_{load} and V, the selection between the input split and the compound split modes is decided based on the maximum power-weighted efficiency η_{HEV} value between the two modes, thus obtaining the resulting mode map in Fig. 5.

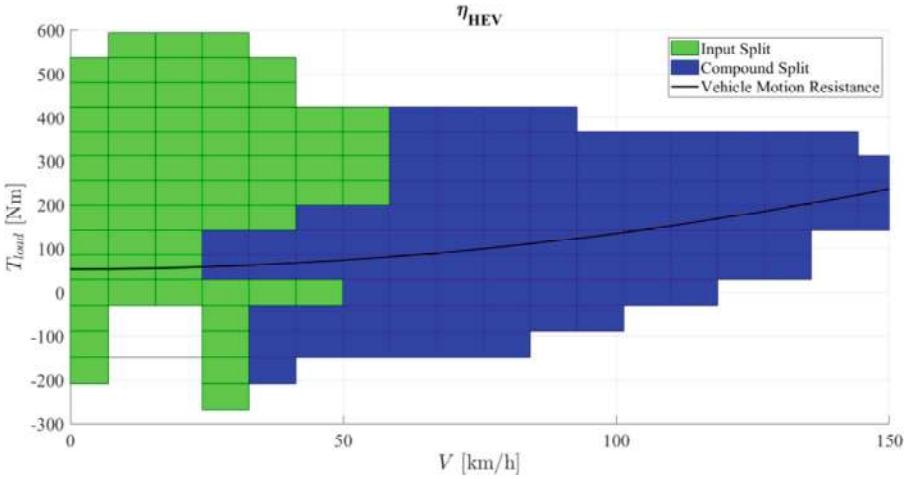

Fig. 5. Resulting powertrain mode map for the EVT 2-mode hybrid system.

The input split mode provides better power-weighted efficiency values for high load torque requests at lower vehicle speeds (launching conditions, uphill motion) meanwhile the compound slit mode is more suitable for high vehicle speeds operating points.

5 Conclusions

This paper shows the way to select the correct mode of a multimode hybrid powertrain through the principle of the power-weighted efficiency, by providing the case study of the EVT 2-mode hybrid system produced by General Motors. The power-weighted efficiency represents a unique global indicator that incorporates the contribution of each mechanical actuators based on the requested power-flow for each powertrain mode. The torque distribution among the powertrain actuators is evaluated to achieve the desired vehicle dynamics, identified by the transmission output shaft acceleration $\dot{\omega}_{out,ref}$, and to satisfy the Charge-Sustaining (extended battery range) or the Charge-Depleting (maximum power-weighted efficiency) targets. Results demonstrate that the methodology represents a powerful tool to select the more suitable powertrain mode for each power request at the transmission output in terms of loading torque and vehicle speed. In the specific case of EVT 2-mode hybrid system, the input split mode represents the best choice for the vehicle launching conditions (high loading torques and low vehicle speeds) meanwhile the compound split mode is preferred to guarantee the same efficiency level at higher vehicle speeds.

References

1. Goal 11: Make cities inclusive, safe, resilient and sustainable. https://www.un.org/sustainabledevelopment/cities/

2. Mi, C., Masrur, M.A.: Hybrid Electric Vehicles: Principles and Applications with Practical Perspectives. Wiley, Hoboken (2017)
3. Ehsani, M., Gao, Y., Longo, S., Ebrahimi, K.M.: Modern Electric, Hybrid Electric, and Fuel Cell Vehicles. CRC Press, Boca Raton (2018)
4. Bole, B., Coogan, S., Cubero-Ponce, C., Edwards, D., Melsert, R., Taylor, D.: Energy management control of a hybrid electric vehicle with two-mode electrically variable transmission. In: EVS26 International Battery, Hybrid and Fuel Cell Electric Vehicle Symposium, pp. 6–9, May 2012
5. Galvagno, E., Vigliani, A., Velardocchia, M.: Transient response and frequency domain analysis of an electrically variable transmission. Adv. Mech. Eng. **10**(5) (2018)
6. Zhang, X., Peng, H., Sun, J.: A near-optimal power management strategy for rapid component sizing of multimode power split hybrid vehicles. IEEE Trans. Control Syst. Technol. **23**(2), 609–618 (2014)
7. Zhang, X., Eben Li, S., Peng, H., Sun, J.: Efficient exhaustive search of power-split hybrid powertrains with multiple planetary gears and clutches. J. Dyn. Syst. Measur. Control **137**(12), 121006 (2015)
8. Zhuang, W., Zhang, X., Ding, Y., Wang, L., Hu, X.: Comparison of multi-mode hybrid powertrains with multiple planetary gears. Appl. Energy **178**, 624–632 (2016)
9. Guercioni, G.R., Galvagno, E., Tota, A., Vigliani, A.: Adaptive equivalent consumption minimization strategy with rule-based gear selection for the energy management of hybrid electric vehicles equipped with dual clutch transmissions. IEEE Access **8**, 190017–190038 (2020)
10. Sciarretta, A., Back, M., Guzzella, L.: Optimal control of parallel hybrid electric vehicles. IEEE Trans. Control Syst. Technol. **12**(3), 352–363 (2004)
11. Delprat, S., Lauber, J., Guerra, T.M., Rimaux, J.: Control of a parallel hybrid powertrain: optimal control. IEEE Trans. Veh. Technol. **53**(3), 872–881 (2004)
12. Kim, N., Cha, S., Peng, H.: Optimal control of hybrid electric vehicles based on Pontryagin's minimum principle. IEEE Trans. Control Syst. Technol. **19**(5), 1279–1287 (2010)
13. Guercioni, G.R., Vigliani, A., Rizzoni, G.: Dynamic programming solution for the energy management problem in HEVs equipped with DCTs. Int. J. Autom. Technol. (in print)
14. Grewe, T.M., Conlon, B.M., Holmes, A.G.: Defining the general motors 2-mode hybrid transmission (no. 2007-01-0273). SAE technical paper (2007)
15. Tinelli, V., Galvagno, E., Velardocchia, M.: Dynamic analysis and control of a dual mode electrically variable transmission. In: Uhl, T. (ed.) Advances in Mechanism and Machine Science: Proceedings of the 15th IFToMM World Congress on Mechanism and Machine Science, pp. 3731–3740. Springer, Cham (2019). https://doi.org/10.1007/978-3-030-20131-9_368
16. Guercioni, G.R., Galvagno, E., Tota, A., Vigliani, A., Zhao, T.: Driveline backlash and half-shaft torque estimation for electric powertrains control (no. 2018-01-1345). SAE technical paper (2018)
17. Serrao, L., Onori, S., Rizzoni, G.: A comparative analysis of energy management strategies for hybrid electric vehicles. J. Dyn. Syst. Measur. Control **133**(3), 031012 (2011)
18. Galvagno, E., Tota, A., Vigliani, A., Velardocchia, M.: Pressure following strategy for conventional braking control applied to a HIL test bench. SAE Int. J. Passeng. Cars-Mech. Syst. **10**(2017-01-2496), 721–727 (2017)